Journal of the Korean Crystal Growth and Crystal Technology
Vol. 16, No. 4 (2006) 133-140

Fluoride single crystals for UV/VUV nonlinear optical applications

Kiyoshi Shimamura†, Encarnación G. Víllora, Kenichi Muramatsu*, Kenji Kitamura and Noboru Ichinose**

National Institute for Materials Science, Tsukuba 305-0044, Japan
**Nikon Corp., Kanagawa 228-0828, Japan*
***ZAIKEN, Waseda University, Tokyo 169-0051, Japan*

(Received November 4, 2005)
(Accepted April 11, 2006)

Abstract The growth characteristics and properties of large size $SrAlF_5$ single crystals are described and compared with those of $BaMgF_4$. Transmission spectra in the vacuum ultraviolet wavelength region indicate a high transparency of $SrAlF_5$ (about 90 % without considering surface reflection loses) down to 150 nm, on contrast to the optical loses observed for $BaMgF_4$. The ferroelectric character of $SrAlF_5$ is evidenced by the reversal of the spontaneous polarization in a hysteresis loop. The higher potential of $SrAlF_5$ in comparison with $BaMgF_4$ for the realization of all-solid-state lasers in the ultraviolet wavelength region by the quasi-phase matching (QPM) technique is pointed out. $SrAlF_5$, besides a higher grade of transparency, shows a nonlinear effective coefficient similar to that of quartz and uniaxial nature, on contrast to the one order smaller nonlinear coefficient and biaxial character of $BaMgF_4$. The refractive index of $SrAlF_5$ from the ultraviolet to the near-infrared wavelength region is measured by the minimum deviation method. The Sellmeier and Cauchy coefficients are obtained from the fits to the curves of the ordinary and extraordinary refractive indices, and the grating period for the first order QPM is estimated as a function of the wavelength. The poling periodicity for 193 nm SHG from 386 nm is 4 μm.

Key words Fluoride, $SrAlF_5$, $BaMgF_4$, Ferroelectric, Nonlinear optics, UV, SHG

1. Introduction

All solid-state lasers (ASSL) emitting from the infrared (IR) to the near ultraviolet (UV) have been well-established over the past decades. Second-, third- and fourth- harmonic generation are realized by the birefringent phase matching (BPM) of oxide nonlinear crystals such as β-BaB_2O_4 (BBO), $CsLiB_6O_{10}$ (CLBO), LiB_3O_5 (LBO) and $Li_2B_4O_7$. These crystals, however, can be used only for wavelengths over 200 nm, as indicated in Table 1. At present, excimer lasers, namely KrF (248 nm) and ArF (193 nm), are used as the coherent light sources in the UV wavelength region. Unfortunately, these present several disadvantages such as a fast degradation, a high toxicity and a low beam quality. There is therefore a strong demand on ASSL in the UV and vacuum ultraviolet (VUV) for industrial use in steppers for optical lithography and diverse medical applications. The lack of optical grade nonlinear crystals transparent into the UV/VUV, as well as a large Poynting vector walk-off inherent to the BPM at short wavelengths, have made impossible the second-harmonic generation (SHG) in the UV/VUV.

Table 1
Oxide crystals used for BPM SHG

crystal	absorption edge [nm]	limit for BPM SHG [nm]
LBO	160	277
CLBO	180	236
BBO	189	205

†Corresponding author
Tel: +81-29-860-4692
Fax: +81-29-851-6159
E-mail: shimamura.kiyoshi@nims.go.jp

A new approach, the quasi-phase matching (QPM), which was theoretically already predicted in the 60's [1], is being developed since the beginning of the 90's [2]. By this method, the frequency conversion is obtained by the use of a ferroelectric crystal, which has been periodically poled (PP) in μm order domains. SHG by QPM has been shown in well-known crystals, such as $LiNbO_3$ or $LiTaO_3$ [3]. These crystals, however, can also not be used in the UV/VUV wavelength region, since their cutoff wavelengths lie in the near UV at 330 and 280 nm, respectively.

In the search for more transparent materials among the pyroelectric fluoride $BaMF_4$ family (M = Mg, Mn, Fe, Co, Ni, Zn), $BaMgF_4$ and $BaZnF_4$ have been focus of attention since they are colorless and transparent down to < 150 nm. These compounds are isomorphous, crystallizing in the orthorhombic system with space group $Cmc2_1$ [4]. Their pyroelectric and piezoelectric properties have been reported [5]. Ferroelectricity, evidenced by the reversal of the spontaneous polarization

in the case of compounds whose Curie temperature would lie above the melting point [6], has been demonstrated in $BaMF_4$ compounds, except for M = Mn and Fe, by means of the pulse-switching method [7]. They show high coercive fields > 50 kV/cm and spontaneous polarizations about 8 $\mu C/cm^2$. $BaMgF_4$ is a host crystal, which can be doped with transition metal (TM) and rare earth (RE) for solid state laser applications [8, 9]. The ferroelectric properties of thin films of $BaMgF_4$ have been investigated for memory applications, using metal-ferroelectric-semiconductor field-effect transistors [10, 11]. PP of $BaMgF_4$ has been already obtained [12], however, to our knowledge no SHG emission could be observed to date. Further, $BaMgF_4$ is an optically biaxial crystal, exhibits a decreasing transparency in the UV/VUV wavelength region and a relatively small nonlinear coefficient, $d_{eff} \approx 0.06$ pm/V [12]. All these properties are detrimental for the practical use of $BaMgF_4$ in QPM.

$SrAlF_5$ is another fluoride compound, which has been shown to be transparent between 0.16 and 10 μm approximately [13]. Among the literature, there is a controversy about the assignment of the crystalline space group. Initially, Mühll *et al.* suggested by single-crystal diffraction analysis, that to a first approximation the space group is the noncentrosymmetric $I4$, although in fact a small distortion along the *c* axis doubles the *c* parameter, the space group becoming $P4$ [14], which is also noncentrosymmetric. On the contrary, Meehan and Wilson indicated the centrosymmetric space group $I4_1/a$, which excludes any ferroelectric properties [13]. Later, on the basis of the $I4$ space group, Abrahams *et al.* showed that a structure of opposite polarity can be obtained by atomic displacements no greater than about 0.05 nm along the *c* axis, and predicted by it a ferroelectric-paramagnetic phase transition temperature at about 685 K and an estimated spontaneous polarization in the range 9~48 $\mu C/cm^2$ [15]. More recently, Kubel *et al.* have suggested again the $I4_1/a$ space group [16], as well as a new centrosymmetric modification $P2_1/n$ [17]. The difficulties encountered in the determination of space group by diffraction methods are presumably enhanced by the lack of high quality crystals, however, the observation of SHG in powder samples after irradiation with a laser beam have given evidence for a noncentrosymmetric group [15, 18].

In the present work, the growth characteristics of large $SrAlF_5$ and $BaMgF_4$ by the Czochralski (CZ) technique are discussed. The ferroelectric character of $SrAlF_5$ is evidenced by the polarization reversal in a hysteresis loop. $SrAlF_5$ exhibits a high transparency in the UV/VUV wavelength region down to the absorption edge at about 150 nm, whereas $BaMgF_4$ presents large optical loses on scattering centers. An oriented prism was cut and polished from a grown $SrAlF_5$ single crystal. The refractive index of $SrAlF_5$ was then determined for the first time by the minimum deviation method. The Sellmeier and Cauchy coefficients were obtained from the curve fits. Further, the grating period for domain poling in the QPM technique was estimated as a function of the wavelength. The 193 nm ASSL generation is discussed.

2. Experiment

Crystal growth was carried out in a CZ system with a 30 kW R.F.-generator. High purity powders (> 99.99 %) of commercially available SrF_2, AlF_3, BaF_2 and MgF_2 powders were utilized. BaF_2 and MgF_2 were weighted and mixed in stoichiometric composition, while in the case of SrF_2 and AlF_3, the amount of AlF_3 was over the stoichiometric value, in order to compensate for the loses of AlF_3 caused by evaporation from the melt during the growth. Purification of the raw materials was carried out in a Pt crucible, heating at 700°C for a period of 12 hours under vacuum ($\approx 10^{-3}$ Pa). This vacuum level, obtained by a rotary and a diffusion pump, was necessary to eliminate effectively the water and oxygen present in the chamber and raw materials, since even traces of those are well-known to be very detrimental for the optical quality of fluoride crystals. Subsequently, high purity CF_4 gas (99.99 %) was slowly flowed into the furnace and the powders were melted. $BaMgF_4$ and $SrAlF_5$ melt congruently at 920 and 880°C, respectively [13, 19]. After seeding, crystal rotation rate was fixed at 10 rpm, and the pulling rate was varied between 1 and 3 mm/h. Crystals of 1 inch in diameter and several centimeter long were grown.

Transmission spectra were measured under vacuum ($\approx 10^{-1}$ Pa) using a VUV spectrometer, VUV200XY. Ferroelectric properties were measured on a (0 0 1) oriented platte by the virtual-grand method, with Au electrodes sputtered on both sample surfaces. Maximum applied voltages were 100, 150 and 200 V, at 0.1 Hz.

SHG was performed with a Q-SW pulsed Nd : $Y_3Al_5O_{12}$ (Nd : YAG) laser from Sure Lite. Crystals were grinded in a mortar and subsequently irradiated with the 1064 nm laser emission, a 10 Hz repetition rate and ≈ 10 mW.

The refractive index as a function of the wavelength

Table 2
Measured extraordinary and ordinary refractive indices of $SrAlF_5$, n_e and n_o, respectively, by the minimum deviation technique

Atom	Wavelength [nm]	n_o	n_e	Δn
He	1083.025	1.416530	1.417371	0.000841
Hg	924.310	1.417249	1.418191	0.000942
Hg	797.870	1.418497	1.419367	0.000870
Hg	745.433	1.419062	1.419934	0.000872
He	706.519	1.419594	1.420467	0.000872
He	667.815	1.420130	1.420992	0.000862
H	656.273	1.420288	1.421166	0.000878
Cd	643.847	1.420490	1.421372	0.000882
Hg	576.959	1.421687	1.422422	0.000735
Hg	546.074	1.422422	1.423312	0.000891
Hg	546.074	1.422456	1.423343	0.000887
Cd	508.582	1.423461	1.424381	0.000920
Cd	508.582	1.423670	1.424595	0.000926
H	486.133	1.424194	1.425097	0.000903
Cd	479.992	1.424597	1.425526	0.000929
Cd	467.815	1.425079	1.425988	0.000909
Hg	435.835	1.426290	1.427209	0.000919
Hg	404.656	1.427988	1.428916	0.000928
Hg	365.015	1.430820	1.431765	0.000946
Cd	361.051	1.431330	1.432292	0.000962
Cd	346.620	1.432688	1.433644	0.000956
Cd	340.365	1.433333	1.434293	0.000960
Cd	326.106	1.434941	1.435911	0.000970
Hg	313.155	1.436453	1.437430	0.000978
Hg	296.728	1.438905	1.439900	0.000994
Hg	253.652	1.449242	1.451358	0.002116
Cd	228.802	1.456744	1.457851	0.001107
Hg	184.949	1.483488	1.484777	0.001289

was measured by the minimum deviation technique, using discrete emission lines of different atoms (listed in Table 2). For it, a $SrAlF_5$ single crystal was cut and fine polished as a equilateral triangle prism, with the vertical axis coincident with the crystallographic *c* axis. The prism dimensions were: 10 mm height, 6 mm base and a 59.94767° vertical angle.

3 Results and Discussion

3.1. Crystal growth

Figure 1 shows the first $BaMgF_4$ crystal. It was grown at a pulling rate of 3 mm/h with a CaF_2 single crystal as a seed. $BaMgF_4$ growth direction corresponds with the *c* axis. In general, it was observed that crystal growth along this axis, even when $BaMgF_4$ was used as single crystal seed, led to cracking of the grown crystal at the middle part during the cooling process. When, the growth orientation was changed to the *a* axis, single

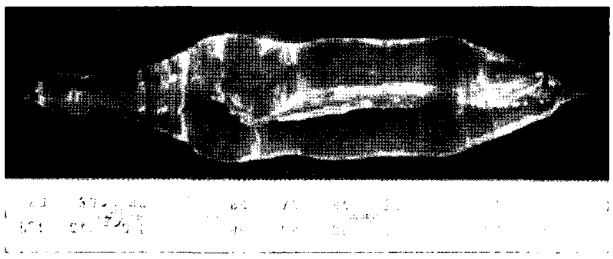

Fig. 1. $BaMgF_4$ crystal grown at a pulling rate of 3 mm/h, using a CaF_2 single crystal as seed. The growth direction was found to be the *c* axis.

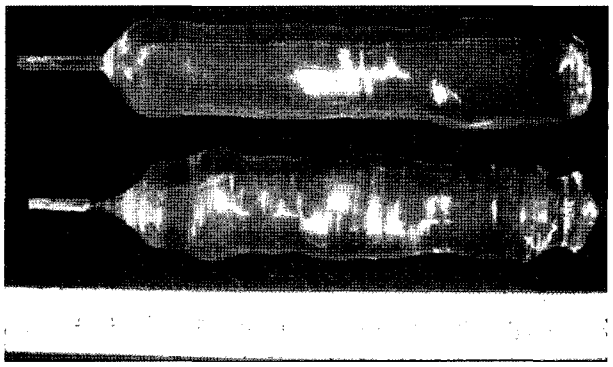

Fig. 2. $BaMgF_4$ single crystals grown along the *a* axis and pulling rates of 3 and 1 mm/h for the upper and lower crystal, respectively.

crystals of 1 inch in diameter could be obtained without cracks as shown in Fig. 2. Although they were transparent, they had a slightly milky appearance caused by light scattering. With decreasing pulling speed from 3 to 1 mm/h, upper and lower crystal respectively, the amount of scattering centers could be reduced considerabley, however, not suppressed completely.

In the case of $SrAlF_5$, we found that only white ceramics could be pulled up when the starting composition was a stoichiometric. Ceramics also appeared on the surface of a growing crystal as soon as the melt composition shifted to the SrF_2 rich side after the evaporation of AlF_3. By a sufficient AlF_3 enrichment of the melt, namely 2 mol%, a cracked boule of transparent $SrAlF_5$ crystals could be pulled up with a Pt wire, as shown in Fig. 3. The use of a CaF_2 seed was avoided, since presumably the seed would react with the melt to form $CaAlF_5$, and therefore it would detach from the melt. Figure 4 shows a crystal of 1 inch in diameter, pulled at a rate of 2.5 mm/h from a 10 mol% AlF_3 enriched melt. Although same cracks are observed, the single crystalline boule is quite large and completely transparent. Figure 5 shows a $SrAlF_5$ single crystal grown with a highly AlF_3 enriched melt and a pulling rate of 1 mm/h. This large deviation from the stoichiometric

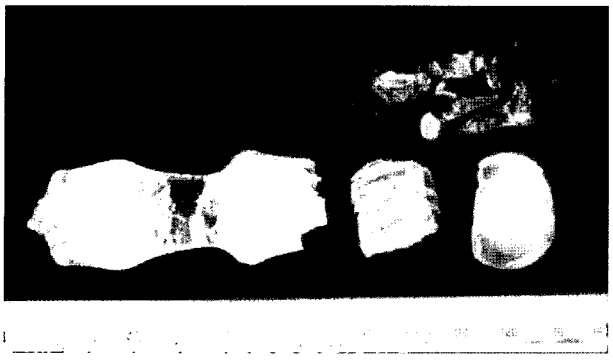

Fig. 3. $SrAlF_5$ crystal grown at a pulling rate of 2.5 mm/h from a 2 mol% AlF_3 enriched melt, using a Pt wire as seed. The growth direction was found to be the *c* axis.

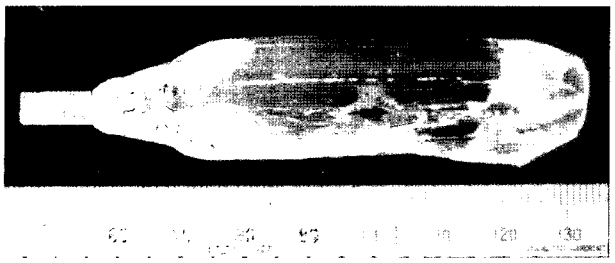

Fig. 4. $SrAlF_5$ crystal grown at a pulling rate of 2.5 mm/h from a 10 mol% AlF_3 enriched melt, using a *c* axis oriented $SrAlF_5$ single crystal seed.

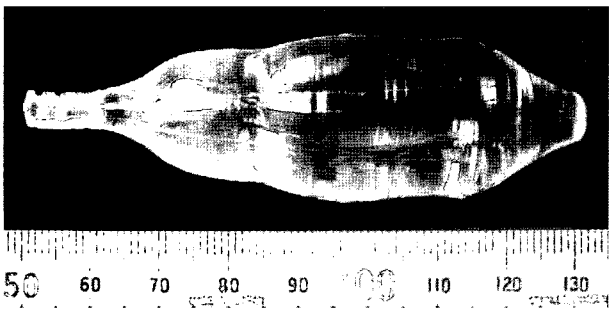

Fig. 5. $SrAlF_5$ single crystal grown along the *c* axis at a pulling rate of 1 mm/h, a rotation speed of 10 rpm and 40 mol% AlF_3 enriched melt.

value did not affect adversely the growth conditions, instead it favored the single crystal growth without cracks by decreasing the pulling speed. This crystal was highly tranparent and no scattering centers could be observed by illuminating it with a laser diode pointer.

3.2. Crystal properties

Figure 6 shows the transmission spectra in the UV/VUV wavelength region of the $BaMgF_4$ and $SrAlF_5$ single crystals shown in the Figs. 2 and 4. In the case of $BaMgF_4$, it is found that the scattering centers, which

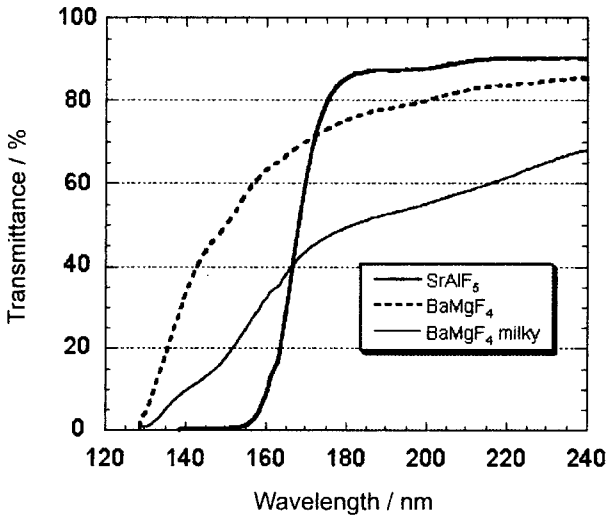

Fig. 6. UV/VUV transmission spectra of as-grown $BaMgF_4$ and $SrAlF_5$ single crystals of the Figs. 2 and 4, respectively. Reflection loses have not been subtracted and the sample thickness, 5.23 mm, was equal for all three samples.

cause the milky appearance of the crystals, are the origin for a monotonous decrease in transparency towards the absorption edge, which lies at ≈ 130 nm. The crystal grown at 3 mm/h shows a lower transmittance than the one grown at 1 mm/h, indicating a larger amount of scattering centers. These results are in accordance with previous observations, which indicated a decay in transparency from about 65 % at 193 nm to about 50 % at 157 nm [12]. On the contrary, $SrAlF_5$ exhibits a high degree of transparency, about ≈ 90 % without considering surface reflection loses, up to the cutoff wavelength at ≈ 155 nm.

Although the second-order nonlinear coefficients of $SrAlF_5$ have not been determined yet, the SHG was confirmed after irradiation with the 1064 nm line of a Nd : YAG laser. Frequency doubled emission intensity at 532 nm, as observed by naked eye, was comparable to that of SiO_2 powder, while the emission from $BaMgF_4$ powder was much weaker, in very good agreement with previous reports [15, 18].

$SrAlF_5$ has been suggested to belong to the class of uniaxial ferroelectrica [15, 20], the polarization reversal taking place predominantly through atomic displacements along the polar axis, namely the *c* axis. The hysteresis loops shown in Fig. 7 evidence for the first time the ferroelectric character of $SrAlF_5$. 100, 150 and 200 V were the maximum voltages applied to a (0 0 1) oriented single crystal plate of 0.18 mm thickness. The rounded shape of the loops indicates the presence of an electric current component, probably caused by a current leakage at the edge due to the small sample thick-

ness. We presume that the hysteresis curve is not yet saturated at 200 V, and therefore from present measurements it can not be concluded which are the values for the coercive field and the spontaneous polarization.

3.3 Refractive index

The crystal in Fig. 5 was cut and fine polished in the prism shown in Fig. 8, and subsequently used for the determination of the refractive index. The results obtained by the minimum deviation technique are summarized in Table 2 and illustrated in Fig. 9. Both the ordinary, n_o, and the extraordinary, n_e, curves were fitted by the Sellmeier's and Cauchy's equations, which are expressed as follows:

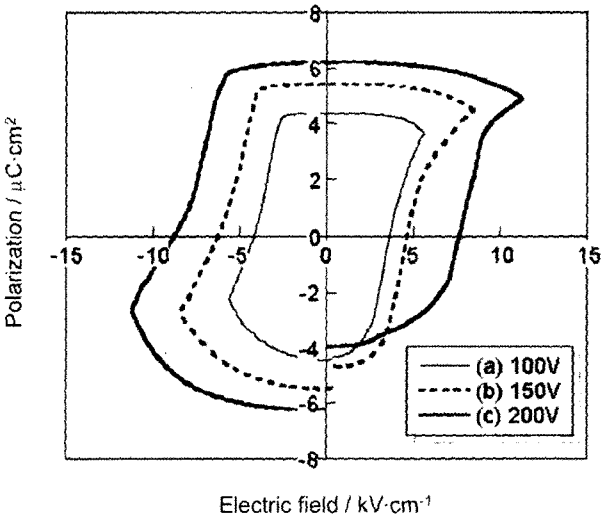

Fig. 7. Polarization hysteresis loops of a (0 0 1) oriented $SrAlF_5$ plate of 0.18 mm thickness. The maximum applied voltages were (a) 100, (b) 150 and (c) 200 V, with a frequency of 0.1 Hz.

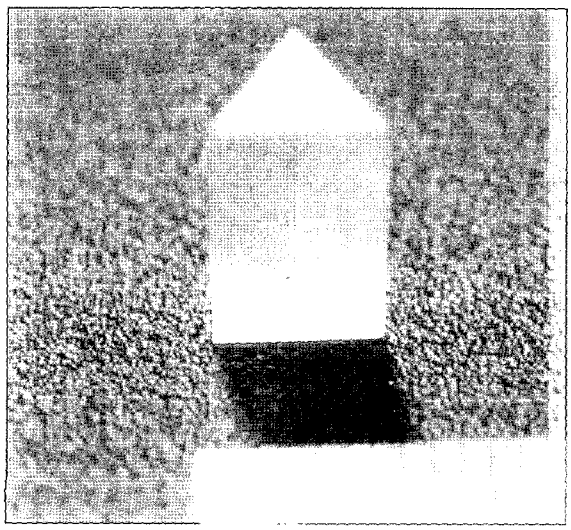

Fig. 8. $SrAlF_5$ single crystal prism cut and polished from the crystal in Fig. 5.

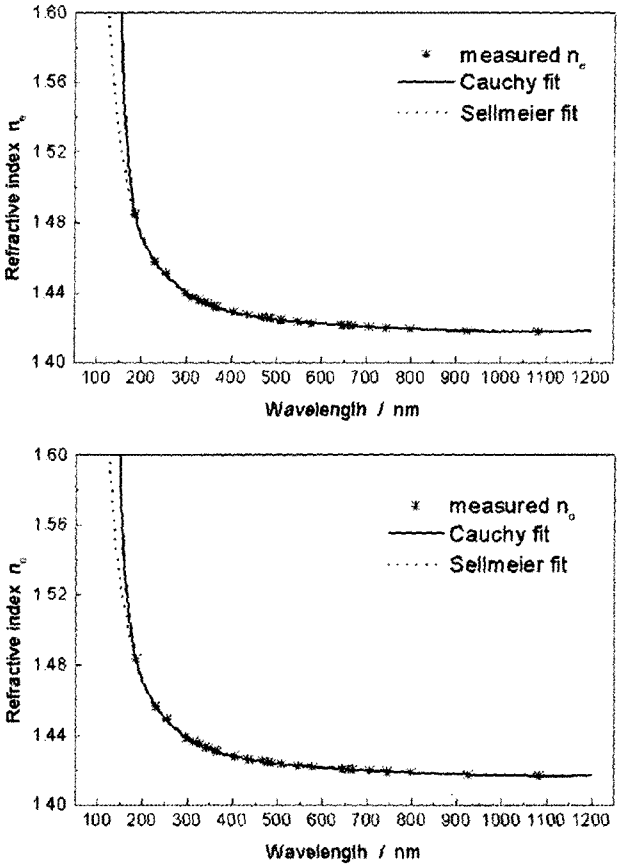

Fig. 9. Measured extraordinary and ordinary refractive indices of $SrAlF_5$, n_e and n_o, respectively, and the calculated curve fits with the Sellmeier and Cauchy equations, Eqs. (1) and (2), respectively. The corresponding fitting coefficients are given in Table 3.

$$\text{Sellmeier: } n^2 = 1 + \frac{A\cdot\lambda^2}{\lambda^2 - B} \tag{1}$$

$$\text{Cauchy: } n^2 = A_0 + A_1\cdot\lambda^2 + \frac{A_2}{\lambda^2} + \frac{A_3}{\lambda^4} + \frac{A_4}{\lambda^6} + \frac{A_5}{\lambda^8} + A_6\cdot\lambda^4 \tag{2}$$

In the measured range, both the Sellmeier and the Cauchy equations can fit very well the experimental values. The obtained fitting parameters are summarized in Table 3. The extrapolations to the short wavelength region, however, indicate that in this region the Cauchy fit is more realistic than the Sellmeier one, because the latter would imply that the material is transparent at wavelengths shorter than the absorption edge, as can be observed in Fig. 9 with a finite refractive index around 150 nm. The Sellmeier equation, with a single pole corresponding to a single resonance frequence, is not accu-

Table 3
Sellmeier and Cauchy coefficients obtained from the fitting of measured refractives indices (Table 2) with the Sellmeier and Cauchy equations, Eqs. (1) and (2), respectively. The corresponding curves are shown in Fig. 9

Equation	Parameter	n_e	n_o
Sellmeier	A	1.0060 ± 0.0003	1.0036 ± 0.0002
	B	$(56.3 \pm 0.3) \times 10^{-4}$	$(59.6 \pm 0.2) \times 10^{-4}$
Cauchy	A_0	2.044 ± 0.010	2.022 ± 0.005
	A_1	−0.056 ± 0.016	−0.028 ± 0.008
	A_2	−0.004 ± 0.002	0.0014 ± 0.0013
	A_3	$(1.1 \pm 0.3) \times 10^{-3}$	$(0.45 \pm 0.15) \times 10^{-3}$
	A_4	$(-4.8 \pm 1.3) \times 10^{-5}$	$(-1.8 \pm 0.7) \times 10^{-5}$
	A_5	$(0.8 \pm 0.2) \times 10^{-6}$	$(0.28 \pm 0.11) \times 10^{-6}$
	A_6	0.024 ± 0.008	0.012 ± 0.004

rate enough at short wavelengths. The refractive indices for the extraordinary wave are larger than those of the ordinary wave, therefore, $SrAlF_5$ is an optically uniaxial positive crystal.

The grating periods required for the first order QPM SHG were calculated from the refractive indices at the fundamental and the second-harmonic wavelengths as follows:

$$p_{33} = \frac{\lambda_\omega}{2[n_{e_{2\omega}} - n_{e_\omega}]} \tag{3}$$

$$p_{31} = \frac{\lambda_\omega}{2[n_{e_{2\omega}} - n_{o_\omega}]} \tag{4}$$

whereas p_{33} and p_{31} are related to the nonlinear coefficients, d_{33} and d_{31}, respectively. The calculated curves are illustrated in Fig. 10. In the UV and visible wavelength regions the Sellmeier and Cauchy fits led to very similar results, instead, in the IR wavelength region, far from the pole, the periods derived from the Sellmeier fit are more accurate, since in this region the Cauchy equation is only an approximation of the Sellmeier one. The grating periods at some definite wavelengths are summarized in Table 4.

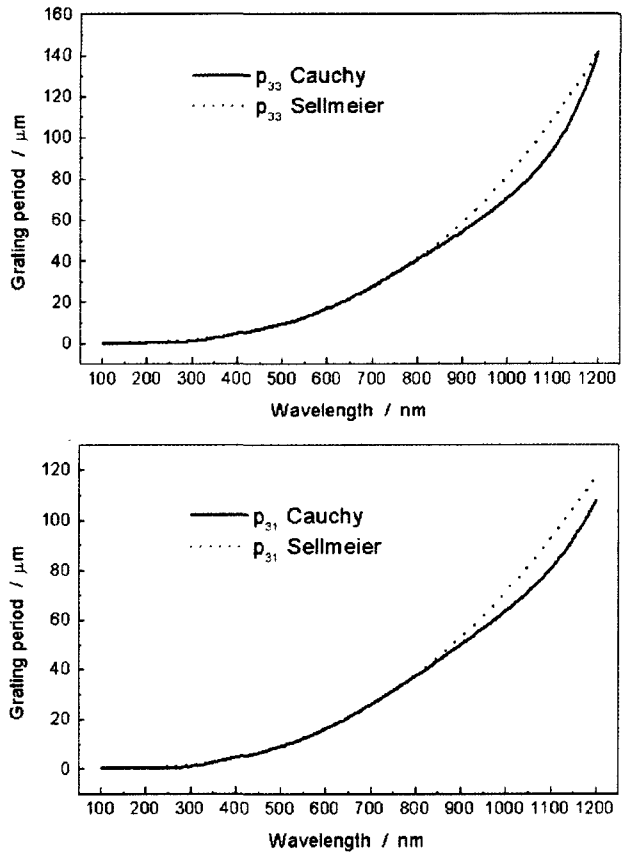

Fig. 10. Grating periods of $SrAlF_5$ for first order QPM as a function of the wavelength. The periods p_{33} and p_{31} correspond to the nonlinear coefficients, d_{33} and d_{31}, respectively. These are calculated with Eqs. (3) and (4), making use of the refractive indices calculated by Eqs. (1) and (2) with the coefficients in Table 3.

Table 4
Grating periods of $SrAlF_5$ for first order QPM at definite wavelengths. The p_{33} and p_{31} periods are obtained from Fig. 10 and correspond to the nonlinear coefficients d_{33} and d_{31}, respectively

Wavelength [nm]	Cauchy		Sellmeier	
	p_{33} [μm]	p_{31} [μm]	p_{33} [μm]	p_{31} [μm]
386	4.151	4.082	3.995	3.912
532	11.270	10.856	11.407	10.988
1064	84.624	73.872	97.705	85.593

3.4. Discussion

Table 5 compares some properties of $SrAlF_5$ with those of $BaMgF_4$, since these two materials are at present the most promising for UV/VUV ASSL generation. Although the cutoff wavelength of $SrAlF_5$ is at a longer wavelength than that of $BaMgF_4$, the higher degree of transparency of $SrAlF_5$ is remarkable. Optical loses at the fundamental and/or second-harmonic wavelength are very detrimental for the conversion efficiency. In particular, it should be noticed the potential of $SrAlF_5$ to substitute present ArF laser at 193 nm, as well as its

Table 5
Comparison between $SrAlF_5$ and $BaMgF_4$

	$SrAlF_5$	$BaMgF_4$	Reference
Symmetry	uniaxial	biaxial	[20]
Cutoff wavelength [nm]	≈ 155	≈ 126	
Transmittance at 193 nm [%]	90	60~70	
Nonlinear coefficient [d/d_{11} SiO_2]	≈ 1	0.13	[22]
Coercive field E_c [kV/cm]	< 50	95	[11]
Curie temperature [°C]	442	990	[21]

Table 6
Possible steps to generate 193 nm ASSL radiation

1554 nm	→ 772 nm	→ 386 nm	→ 193 nm
IR laser diodes	N.C.BPM LBO Ti:sapphire laser	C.BPM LBO QPM LN or LT UV laser diodes	QPM $SrAlF_5$

applicability at 177 nm for the mixing of the second and fourth harmonic of a standard Nd : YAG laser, 532 and 266 nm, respectively. The uniaxial characteristic of $SrAlF_5$ is a further advantage, because the anisotropy of the refractive index complicates the determination of the QPM parameters and its practical realization. Concerning the second-order nonlinear coefficient, the largest value for $BaMgF_4$ is quite small, while the effective nonlinear coefficient of $SrAlF_5$ is comparable to that of quartz. Concerning the ferroelectric properties, more precise measurements are still needed, however, as the estimated Curie temperature of $BaMgF_4$ (990°C [21]) is much higher than that of $SrAlF_5$ (442°C [15]), lying even over the melting point, the polling process of $SrAlF_5$ is expected to be more practicable.

For the 193 nm ASSL generation there are a few practicable ways, which are schematized in Table 6. Initial sources could be IR laser diodes (1554 nm), a tunned Ti:sapphire laser (772 nm), or UV laser diodes (386 nm). The 722 nm SHG can be obtained by a non critical (N.C.) BPM with LBO, while the 386 nm fourth harmonic can be achieved by a critical BPM with LBO or a QPM with LN or LT. Although LN and LT give a N.C.PM, so that no additional beam shape control is required, these crystals exhibit solarization and therefore they can not be used at high irradiation power. The eighth harmonic is approached by the QPM with $SrAlF_5$. The grating period estimated for doubling 386 nm emission is about 4 μm (see Table 4), which is about double of that estimated for $BaMgF_4$ [12].

In the discussion above, $SrAlF_5$ is considered for the substitution of the currently used ArF excimer laser (193 nm) by an ASSL emitting at the same wavelength. So far, $SrAlF_5$ is thought just for the last SHG in the UV wavelength region. However, due to the high degree of transparency of $SrAlF_5$ into the IR wavelength region [23], it is also a potential candidate for SHG at longer wavelengths. The irradiation resistance of $SrAlF_5$ is an issue of future investigations. $SrAlF_5$ could be used as well for the SHG of green light from the fundamental emission at 1064 nm of the Nd : YAG laser. According to Table 4, the grating period of $SrAlF_5$ at 1064 nm is about 3 times larger than that of LN or LT [24], so that the process of domain poling can be realized more precisely. $SrAlF_5$ could be applied also for the 266 nm fourth harmonic generation of Nd : YAG, with a grating period of 11 μm at 532 nm, intead of the BPM of CLBO or BBO. Further, it should be noticed the potential use of $SrAlF_5$ for shorter wavelengths than 193 nm. By the mixing of the second and fouth harmonic of a standard Nd : YAG laser, a 177 nm ASSL source could be achieved.

4. Conclusion

The growth of $SrAlF_5$ and $BaMgF_4$ single crystals with 1 inch in diameter by the CZ technique is described. It is found, that $SrAlF_5$ is highly transparent down to the absorption edge at ≈ 150 nm, in contrast to the relatively low transparency of $BaMgF_4$ in the UV/VUV wavelength region. The nonlinear coefficient has a value similar to that of quartz, with d_{11} = 0.3~0.4 pm/V. The ferroelectric character of $SrAlF_5$ has been demonstrated for the first time by the polarization reversal. Additionally, $SrAlF_5$ is uniaxial and exhibits a larger effective nonlinear coefficient than $BaMgF_4$. The refractive index of $SrAlF_5$ as a function of the wavalength has been determined by the minimum deviation technique. The extraordinary refractive index is larger than the ordinary one, therefore $SrAlF_5$ is an optically uniaxial positive crystal. From the refractive indices of $SrAlF_5$, a 4 μm grating period is calculated for the SHG of 193 nm from 386 nm by the first order QPM technique. All these properties suggest that $SrAlF_5$ is a more promising candidate than $BaMgF_4$ for the realization of ASSL in the UV/VUV wavelength region by the QPM technique, especially for ASSL 193 nm.

References

[1] J.A. Armstrong, N. Bloembergen, J. Duncan and P.S. Pershan, "Interactions between light waves in a nonlinear dielectric", Phys. Rev. 127 (1962) 1918.
[2] M.M. Fejer, G.A. Magel, D.H. Jundt and R.L. Byer, "Quasi-phase-matched second harmonic generation: tuning and tolerances", IEEE J. Quantum Electron. 28 (1992) 2631.
[3] J.P. Meyn and M.M. Fejer, "Tunable ultraviolet radiation by second-harmonic generation in periodically poled lithium tantalate", Opt. Lett. 22 (1997) 1214.
[4] E.T. Keves, S.C. Abrahams and J.L. Bernstein, "Crystal structure of pyroelectric paramagnetic barium manganese fluoride, $BaMnF_4$", J. Chem. Phys. 51 (1969) 4928.

[5] M. Eibschuetz, H.J. Guggenheim, S.H. Wemple, I. Camlibel and M. DiDomenico, "Ferroelectricity in $BaM^{2+}F_4$", Phys. Lett. 29A (1969) 409.
[6] N.W. Ashcroft and N.D. Mermin, "Solid State Physics", Saunders College Publishing (Harcourt College Publishers, USA, 1976).
[7] M. Eibschutz and H.J. Guggenheim, "Antiferromagnetic-piezoelectric crystals : $BaMF_4$ (M = Mn, Fe, Co and Ni)", Solid Sate Commun. 6 (1968) 737.
[8] J.M. Rey, H. Bill, D. Lovy and H. Hagemann, "Europium doped $BaMgF_4$, an EPR and optical investigation", J. Alloys Compd. 268 (1998) 60.
[9] N. Kodama, T. Hoshino, M. Yamaga, N. Ishizawa, K. Shimamura and T. Fukuda, "Optical and structural studies on $BaMgFe_4 : Ce^{3+}$ crystals", J. Cryst. Growth 229 (2001) 492.
[10] T. Hayashi, M. Yoshihara, S. Ohmi and E. Tokumitsu, "Electrical properties of ferroelectric $BaMgF_4$ films grown on GaAs substrates using AlGaAs buffer layer", Appl. Surf. Science 117/118 (1997) 418.
[11] S. Sinharoy, H. Buhay, M.H. Francombe, W.J. Takei, N.J. Doyle, J.H. Fieger, D.R. Lampe and E. Stepke, "Growth and characterization of ferroelectric $BaMgF_4$ films", J. Vac. Sci. Technol. A9 (1991) 409.
[12] S.C. Buchter, T.Y. Fan, V. Liberman, J.J. Zayhowski and M. Rothschild, Periodically polled $BaMgF_4$ for ultraviolet frequency generation", Opt. Lett. 26 (2001) 1693.
[13] J.P. Meehan and E.J. Wilson, "Single crystal growth and characterization of $SrAlF_5$ and $Sr_{1-x}Eu_{2+x}AlF_5$", J. Cryst. Growth 15 (1972) 141.
[14] R, von der Mühll, S. Anderson and J. Galy, "Sur quelques fluometallates alcalino-terreux. 1. Structure cristalline de $BaFeF_5$ et $SrAlF_5$", Acta Cryst. B27 (1971) 2345.
[15] S.C. Abrahams, J. Ravez, A. Simon and J.P. Chaminade, " Ferroelectric behavior and phase transition at 715 K in $SrAlF_5$", J. Appl. Phys. 52 (1981) 4740.
[16] F. Kubel, "The crystal structures of $SrAlF_5$ and $Ba_{0.43(1)}Sr_{0.57(1)}AlF_5$", Z. Anorg. Allg. Chem. 624 (1998) 1481.
[17] M. Weil, E. Zobetz, F. Werner and F. Kuber, "New alkaline earth aluminium fluorides with the formula $(M,M')AlF_5$ (m,M') = Ca, Sr, ba", Solid State Sciences 3 (2001) 441.
[18] J. Ravez, S.C. Abrahams, J.P. Chaminade, A. Simon, J. Granner and P. Hagenmueller, "Ferroelectric behavior and phase transitions in the $SrAlF_5$ family", Ferroelectrics 38 (1981) 773.
[19] M. Rolin and M. Clausier, "Le systeme fluorure de calcium fluorure de baryum-fluorure de magnèsium", Rev. Int. Hautes Temp. Refract. 4 (1967) 42.
[20] S.C. Abrahams and E.T. Keve, "Structural basis of ferroelectricity and ferroclasticity", Ferroelectrics 2 (1971) 129.
[21] M. DiDomenico, J.M. Eibschuetz, H.J. Guggenheim and I. Camlibel, "Dielectric behavior of ferroelectric $BaMF_4$ above room temperature", Solid State Commun. 7 (1969) 1119.
[22] H.G.J.G. Berman and G.R. Crane, "Linear and nonlinear optical properties of ferroelectric $BaMgF_4$ and $BaZnF_4$", J. Appl. Phys. 46 (1975) 4645.
[23] K. Shimamura, E.G. Víllora, K. Muramatsu and N. Ichinose, "Advantageous growth characteristies and properties of $SrAlF_5$ compared with $BaMgF_4$ for UV/VUV nonlinear optical applications", J. Cryst. Growth (2004).
[24] L. Myers, R. Eckardt, M. Fejer, R. Byer, W. Bosenberg and J. Pierce, "Quasi-phase-matched optical parametric oscillators in bulk periodically poled $LiNbO_3$", J. Opt. Soc. Am. B 12 (1995) 2102.